Electronic and optical properties of γ-Al_2O_3 from *ab initio* theory

2004 J. Phys.: Condens. Matter 16 2891

(http://iopscience.iop.org/0953-8984/16/16/013)

INSTITUTE OF PHYSICS PUBLISHING JOURNAL OF PHYSICS: CONDENSED MATTER

J. Phys.: Condens. Matter **16** (2004) 2891–2900 PII: S0953-8984(04)66689-6

Electronic and optical properties of γ-Al_2O_3 from *ab initio* theory

R Ahuja[1], J M Osorio-Guillen[1], J Souza de Almeida[1], B Holm[1,2], W Y Ching[3] and B Johansson[1,4]

[1] Condensed Matter Theory Group, Department of Physics, Uppsala University, BOX 530, S-751 21, Uppsala, Sweden
[2] Institute for Solid State Physics, University of Tokyo, 5-1-5 Kashiwanoha, Kashiwa, Chiba 277-8581, Japan
[3] Department of Physics, University of Missouri-Kansas City, Kansas City, MO 64110-2499, USA
[4] Applied Materials Physics, Department of Materials Science and Engineering, Royal Institute of Technology, SE-100 44, Stockholm, Sweden

Received 24 July 2003
Published 8 April 2004
Online at stacks.iop.org/JPhysCM/16/2891
DOI: 10.1088/0953-8984/16/16/013

Abstract

We report on a density functional theory calculation of the electronic structure and optical properties of γ-Al_2O_3. We have made a comparison between the optical and electronic properties of the α and γ phases of alumina. The calculated bulk modulus of the γ phase is slightly lower than that of the α phase. The calculated static dielectric function and the optical constant of the γ phase are very close to those of the α phase.

1. Introduction

Modelling of structural, mechanical and optical properties of Al_2O_3 by means of atomistic simulations has become an important tool used for the understanding of the properties of this and other materials during the last few years. Aluminium oxide (corundum) is a most important refractory ceramic material. It is known to exist in several different phases, such as the ones labelled α (hexagonal), β (hexagonal), γ (cubic spinel), η (cubic spinel), θ (monoclinic), κ (orthorhombic), δ (tetragonal) and χ (cubic). In technological applications, for instance in wear-resistant cutting tool materials [1], the most commonly used phase is the stable α phase. However, recent developments of industrial applications of alumina have directed interest to other, meta-stable, phases of alumina, in particular the so-called γ and κ phases. The complicated crystal structure in these cases has provided both experimentalists and theoreticians with new, non-trivial challenges. The task of determining the positions of the constituent atoms in γ-Al_2O_3 has not yet been solved. Experimental difficulties arise due to the meta-stability of the phase, and the associated difficulty of obtaining a significant number of pure samples. Further, there is a poor degree of crystallinity.

The first structural determination of the γ phase was done as long ago as 1935, when Verwey [2] reported the defect spinal structure for this phase. This structure can be described by the formula $Al_{21\frac{1}{3}}O_{32}\circ_{2\frac{2}{3}}$ ($\circ$ = vacancy). However, the question of the vacancy distribution between the tetrahedral and octahedral sites is still an open one. In this regard, *ab initio* simulations can be used to resolve this very important question. On the other hand, there are several conflicting reports from theoretical calculations on this issue. For example, calculations based on classical molecular dynamics (MD) and Monte Carlo simulations in conjunction with *ab initio* calculations show that more than 50% of the vacancies are on tetrahedral sites. However, the calculations of Mo *et al* [3] based on empirical pair potentials in conjunction with the *ab initio* OLCAO method, as well as the classical MD simulations by Streitz and Mintmire [4], suggest that these vacancies occupy octahedral sites.

As has been shown for κ-Al_2O_3 [5], first principles calculations have predicted the correct crystal structure from about 100 different candidate configurations. This prediction was recently confirmed by experiment [6]. We have utilized a corresponding procedure in order to find the lowest energy configuration for γ-Al_2O_3. In this case the situation is more complicated than for κ-Al_2O_3, because of the fractional occupancy of Al. This means that in order to get a complete occupation of Al sites, one needs a very big unit cell consisting of 160 atoms. This will make the calculations extremely time consuming and the possible number of configurations will be very large. Therefore, this problem cannot be handled in a reasonable time. Another possible approach is to use a cubic unit cell with three vacancies, as was shown by one of the co-authors of this paper [3]. In this case there will be 53 atoms with three vacancies. Further, there exists yet another description, which was suggested by Sohlberg *et al* [7], namely the consideration of a primitive cell which has a smaller number of atoms than in the approach suggested by Mo *et al* [3]. In this case one has 16 Al atoms and 24 O atoms, giving the same ratio of Al to O, i.e. 2/3, as that for defect spinel structure suggested by Verwey in 1935. There will result two vacancies which can occupy tetrahedral, octahedral or both tetrahedral and octahedral sites.

In this paper we present some results that follow from the knowledge of the crystal structure of gamma-alumina. In particular the differences as well as the similarities between the γ and α phases are examined.

2. Computational details

In order to study the electronic structure and total energy of γ-Al_2O_3, the full-potential linear muffin-tin-orbital (FPLMTO) method [8] was used. The calculations were based on the local-density approximation (LDA) within density functional theory (DFT), and we used the Hedin–Lundqvist [9] parametrization for the exchange and correlation potential. Basis functions, electron densities, and potentials were calculated without any geometrical approximation [8]. These quantities were expanded in combinations of spherical harmonic functions (with a cut-off $\ell_{max} = 8$) inside non-overlapping spheres surrounding the atomic sites (muffin-tin spheres) and in a Fourier series in the interstitial region. The muffin-tin sphere occupied approximately 55% of the unit cell. The radial basis functions within the muffin-tin spheres are linear combinations of radial wavefunctions and their energy derivatives, computed at energies appropriate to their site and principal as well as orbital atomic quantum numbers, whereas outside the muffin-tin spheres the basis functions are combinations of Neuman or Hankel functions [10, 11]. In the calculations reported here, we made use of pseudo-core 2p and valence band 3s, 3p, and 3d basis functions for Al, and valence band 2s, 2p, and 3d basis functions for O, with two corresponding sets of energy parameters, one appropriate for the semi-core 2p states, and the other appropriate for the valence states. The resulting basis formed a single, fully

hybridized basis set. This approach has previously proven to give a well converged basis [8]. For the sampling of the irreducible wedge of the Brillouin zone we used the special k-point method [12]. We have used 280 k-points in the irreducible part of the Brillouin zone. In order to speed up the convergence we have associated each calculated eigenvalue with a Gaussian broadening with a width of 20 mRyd.

The crystal lattice of the γ phase is very close to that of the spinel $MgAl_2O_4$ structure. The unit cell of $MgAl_2O_4$ is formed by 32 atoms of oxygen in a cubic close packing sequence, 16 aluminium atoms in octahedral sites and eight magnesium atoms in tetrahedral sites. The γ phase of Al_2O_3 differs from the spinel structure in the number of Al atoms. The unit cell contains $21\frac{1}{3}$ Al atoms which are divided onto octahedral and tetrahedral positions, creating $2\frac{2}{3}$ vacancies. If in the $MgAl_2O_4$ structure we replace the Mg atoms by Al atoms as well, we will arrive at 24 Al and 32 O atoms. This gives a formula of Al_6O_8 with three formula units in the unit cell, resulting in a total of 18 Al atoms and 24 O atoms. By removing two Al atoms, one gets the correct stoichiometry, Al_2O_3, with eight formula units, i.e., 40 atoms. The two vacancies can be distributed either purely in tetrahedral sites or in octahedral sites. Furthermore, one can have one vacancy in a tetrahedral and the other in an octahedral site. When considering all possible configurations, the one which has both vacancies on octahedral sites has the lowest total energy. Hence, we have performed electronic and optical calculations for these configurations. A more detailed description is given in our previous work [13].

2.1. Calculation of the dielectric function

The ($q = 0$) dielectric function was calculated in the momentum representation, which requires the matrix elements of the momentum, $\mathbf{p}$, between occupied and unoccupied eigenstates. To be specific the imaginary part of the dielectric function, $\epsilon_2(\omega) \equiv \mathrm{Im}\,\epsilon(\mathbf{q} = 0, \omega)$, was calculated from [14, 15]

$$\epsilon_2^{ij}(\omega) = \frac{4\pi^2 e^2}{\Omega m^2 \omega^2} \sum_{\mathbf{k}nn'\sigma} \langle \mathbf{k}n\sigma | p_i | \mathbf{k}n'\sigma \rangle \langle \mathbf{k}n'\sigma | p_j | \mathbf{k}n\sigma \rangle f_{\mathbf{k}n} (1 - f_{\mathbf{k}n'}) \delta(e_{\mathbf{k}n'} - e_{\mathbf{k}n} - \hbar\omega). \quad (1)$$

In equation (1), e is the electron charge, m the electron mass, Ω is the crystal volume and $f_{\mathbf{k}n}$ is the Fermi distribution function. Moreover, $|\mathbf{k}n\sigma\rangle$ is the crystal wavefunction corresponding to the nth eigenvalue with crystal momentum $\mathbf{k}$ and spin σ. With our spherical wave basis functions, the matrix elements of the momentum operator can be conveniently calculated in spherical coordinates and for this reason the momentum is written as $\mathbf{p} = \sum_\mu \mathbf{e}^*_\mu p_\mu$ [16], where μ is -1, 0, or 1, and $p_{-1} = \frac{1}{\sqrt{2}}(p_x - \mathrm{i}p_y)$, $p_0 = p_z$, and $p_1 = \frac{-1}{\sqrt{2}}(p_x + \mathrm{i}p_y)$.[5]

The evaluation of the matrix elements in equation (1) is done separately over the muffin-tin and the interstitial region. The integration over the muffin-tin spheres is done in a way similar to the procedures used by Oppeneer [17] and Gasche[14]. However, their calculations utilized the atomic sphere approximation (ASA). A fully detailed description of the calculation of the matrix elements is presented elsewhere [18].

The summation over the Brillouin zone in equation (1) is performed by using linear interpolation on a mesh of uniformly distributed points, i.e., the tetrahedron method. Matrix elements, eigenvalues, and eigenvectors are calculated in the irreducible part of the Brillouin zone. The total dielectric function is obtained from the longitudinal ($\|$) and the transverse ($\perp$) components as $\epsilon(\omega) = (\epsilon_\|(\omega) + 2\epsilon_\perp(\omega))/3$. The correct symmetry for the dielectric constant was obtained by averaging the calculated dielectric function. Finally, the real part of

[5] In practice we calculate matrix elements of the symmetrized momentum operator $\langle i|\overleftrightarrow{\mathbf{p}}_\mu|j\rangle \equiv (\langle i|p_\mu j\rangle + (-1)^\mu \langle p_{-\mu} i|j\rangle)/2$.

Table 1. Comparison between the experimental and theoretical crystallographic lattice parameters for Al_2O_3.

	Expt		Calc.	
	γ[a]	α[b]	γ	α
V (Å^3)	371.35	255.04	362.4	253 (258)[c]
b/a	1.0	1.0	1.0	1.0 (1.0)[c]
c/a	1.0	2.73	1.0	2.73 (2.71)[c]
B (GPa)		254.4	232	253.5 (248)[c]

[a] Reference [2].
[b] Reference [31].
[c] Reference [19].

the dielectric function, $\epsilon_1(\omega)$, is obtained from $\epsilon_2(\omega)$ using the Kramers–Kronig relation,

$$\epsilon_1(\omega) \equiv \mathrm{Re}(\epsilon(\mathbf{q}=0,\omega)) = 1 + \frac{1}{\pi}\int_0^\infty \mathrm{d}\omega'\,\epsilon_2(\omega')\left(\frac{1}{\omega'-\omega}+\frac{1}{\omega'+\omega}\right). \quad (2)$$

We have evaluated the above equation setting the frequency cut-off to be four times larger than the highest frequency in the considered frequency range which yields very accurate results.

3. Results and discussion

3.1. Electronic structure

The electronic structure has been calculated within the method described for both α- and γ-Al_2O_3. In this subsection we present a general account for the results. In the case of the α phase there are experimental results available for several quantities, while such are absent for γ-Al_2O_3. Comparison between the theoretical and experimental results for α-Al_2O_3 thus serves to give an indication of the accuracy of our predictions for the γ phase. In table 1, we have shown our calculated volumes of the unit cells of the α and γ phases, as well as their bulk moduli. From the table one finds that agreement is very good for the α phase. Our results are also in agreement with OLCAO calculations by Ouyang and Ching [19]. The bulk modulus of the γ phase is a prediction and its value is a little bit lower than for the α phase.

The calculated density of states (DOS) for α and γ phases is shown in figure 1. For the α phase, soft-x-ray and photo-electron spectrum measurements show an upper valence band (UVB) width of 9.2–9.5 eV [20], polarized-x-ray emission experiments a width around 8 eV [21], while x-ray photoemission measurements show one around 15 eV [22]. The higher experimental width values, as compared to the calculated 7.2 eV, may be due to the broadening processes present in the experiment. We calculate the width of the lower-valence-band (LVB) O 2s density of states (DOS) peak to be 3 eV, located between -19 and -16 eV from the top of the valence band. In the x-ray photoemission experiment this width is 6 eV [22]. This LVB difference may be due to correlation effects in these deep lying semi-core-like states, not accounted for by the LDA. The bottom of the conduction band (CB), i.e., the peak around 10 eV, mainly consists of Al 3s states, and the peak around 15 eV comes from the antibonding O 2p and Al 3p states. The CB also has a fair amount of contribution from Al 3d states. The calculated bandgap for the α phase is 6.6 eV whereas the experimental [23] gap is 8.8 eV. This discrepancy arises, as we have mentioned before, because of the inability of DFT to describe excited states.

For the γ phase, the O 2p and O 2s states are 8.5 and 3.9 eV wide respectively, and separated by a gap of 8.0 eV. The peak in the LVB-band DOS is situated between -20 and

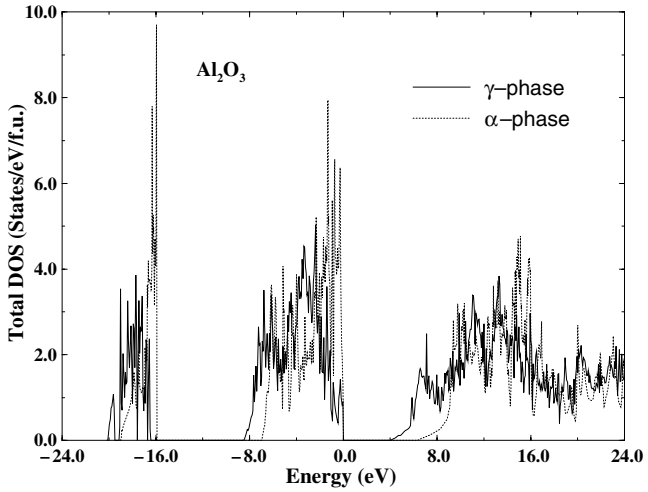

Figure 1. Calculated density of states (DOS) for Al_2O_3 in α phase and γ phase. Fermi energy has been set to zero energy level.

−16 eV from the top of the valence band. Again our calculations are in good agreement with XPS data of Ealet *et al* [24]. Two model calculations by Mo *et al* [3] show that the O 2p and O 2s states are 7.8–8.1 and 3.7–4.1 eV wide respectively. The calculated bandgap for the γ phase is 3.9 eV and calculations by Mo *et al* show between 4.8 and 5.1 eV, while the experimental one is 7.0 eV [24]. Thus, α- and γ-Al_2O_3 have rather similar electron structures. The major differences—in addition to those imposed by the difference in atomic structure—are that γ-Al_2O_3 has slightly broader energy bands, a wider energy gap between the upper and lower valence bands, and a narrower energy gap across the electron-transfer gap, i.e. a bridging of the Fermi level. The overall agreement between experiment and theory for α-Al_2O_3 makes the predictions for γ-Al_2O_3 likely to be rather appropriate.

3.2. Optical properties

From the electronic structure, optical properties of both α- and γ-Al_2O_3 have been calculated by our method. For the α phase there are experimental results for several optical quantities [25], while such are absent for γ-Al_2O_3. In this way a comparison between theoretical and experimental results for α-Al_2O_3 serves to give an indication of the accuracy of our theoretical predictions for the γ phase.

Figures 2 and 3 show the imaginary and real parts of the dielectric functions for the α and γ phases, $\epsilon_2(\omega)$ and $\epsilon_1(\omega)$, respectively. For the α phase our calculated $\epsilon_2(\omega)$ shows two main peaks at around 11 and 15.5 eV and two weak shoulders at around 12.5 and 14 eV, whereas for the γ phase there appear two main peaks at around 10 and 14 eV and one weak shoulder around 15.5 eV. The experimental data for α-Al_2O_3 [25] show interband transitions at 13, 16.5, and 20.5 eV, the latter being a small structure which is absent in our calculated ϵ_2, which shows just a smooth variation in this energy range. For the first two main peaks there is a constant difference between the calculated and experimental positions, mainly because our bandgap is smaller than the experimental one by approximately 2 eV. The scissors operation gives just a rigid shift in $\epsilon_2(\omega)$, leaving the main features of the spectra unchanged, and it decreases $\epsilon_1(\omega)$, which can be seen through the Kramers–Kronig relation. Then if we rigidly shift the calculated curve by 2.0 eV, the calculated spectrum is in good agreement with experiment. However, the

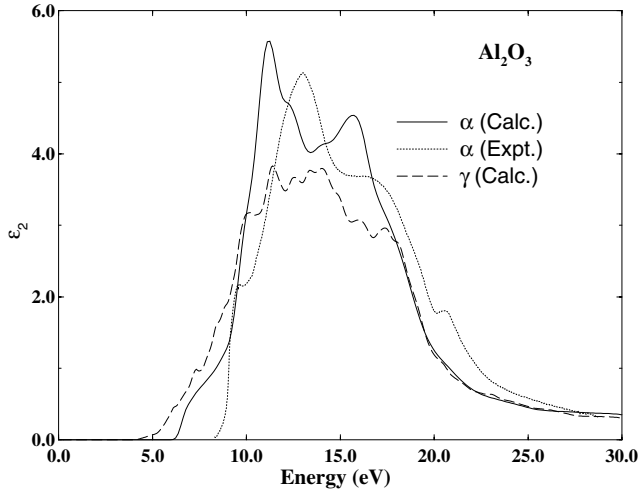

Figure 2. Calculated and experimental imaginary part of the dielectric function, ϵ_2, for α- and γ-Al_2O_3.

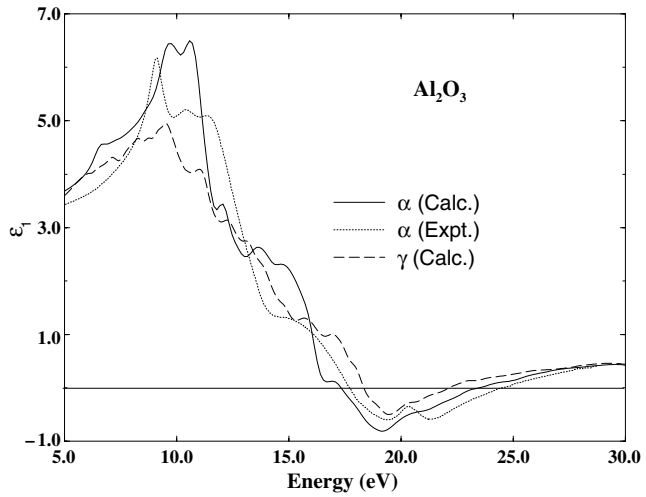

Figure 3. Calculated and experimental real part of the dielectric function, ϵ_1, for α- and γ-Al_2O_3.

steep slope near the absorption edge and the sharp peak in the experimental spectrum are absent in our calculated results. This excitonic peak is missing in our calculated spectra, because our calculations only involve interband transitions from valence- to conduction-band states.

The general behaviour of the γ-Al_2O_3 $\epsilon_2(\omega)$ curve is similar to that for the α phase. In this case, however, the rigid shift should be about 2.7 eV. The origins of the different peaks in the calculated dielectric functions can be traced back to certain terms in the inter-band transitions. Due to selection rules, only transitions that correspond to Δl equal to ± 1 are allowed. From an analysis of the electronic structure of α-Al_2O_3 the first peak at around 11 eV in the calculated spectrum can be explained as due to transitions from Al 3p to Al 3s states. Transitions from Al 3d to Al 3p may give rise to the second main peak at around 15.5 eV.

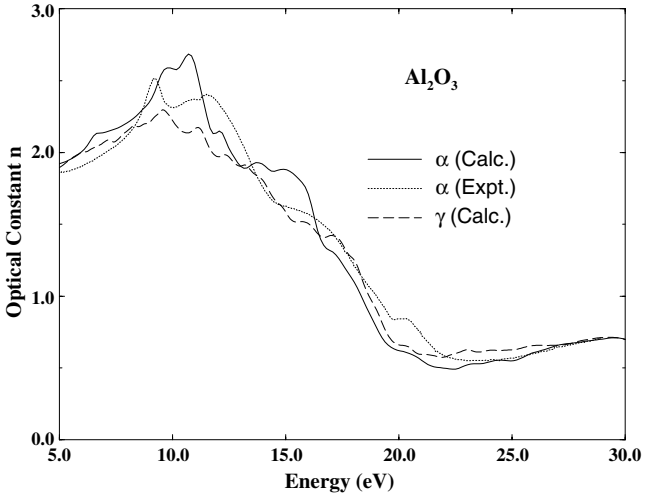

Figure 4. Calculated and experimental optical constant, n, for α- and γ-Al_2O_3.

As before, a Kramers–Kronig (KK) analysis of ϵ_2 yields the real part of the dielectric function, ϵ_1. In figure 3 the calculated ϵ_1 is compared with experimental data. As one can see, all features of the measured data are well reproduced by our calculations. The calculated ϵ_1 curves become negative at 17.3 and 18.2 eV for the α and γ phases, respectively, whereas the experimental α-phase curve crosses the axis at 17.7 eV. In our calculations, it becomes positive again at 23.6 eV for both the α and γ phases, the corresponding experimental value for the α phase being 24.5 eV. In the high energy region, the calculated and measured ϵ_1 curves show very similar behaviour. At the other end of the spectrum, the dielectric function $\epsilon_1(0)$ is calculated to be 3.2 for the α and 3.0 for the γ phase, whereas the experimental α-Al_2O_3 result is 3.1 [26].

The calculated optical constants n and k are shown in figures 4 and 5 together with the experimental data of Arakawa and Williams [25]. Our calculated values of the ordinary refractive index for the α and γ phases are 1.79 and 1.73 respectively, while the measured value by Zouboulis and Grimsditch [27] is 1.77 for the α phase. A previous calculation using the OLCAO method gave an ordinary refractive index of 1.96 [28]. Recently Mo and Ching [29] have done the new KK analysis and found an ordinary refractive index of 1.78. Our present theoretical result and by Mo and Ching [29] for the refractive index is in excellent agreement with experiment. Our calculated spectra in figures 4 and 5 show a good general agreement with experiment, although there are some discrepancies regarding the peak positions, mainly due to errors in the bandgaps which are underestimated by DFT.

We have also calculated the optical reflectivity and conductivity. These we have compared with the recent experimental data of Bortz and French [30]. In figure 6 we show the reflectivity spectrum. The measured spectrum shows an excitonic peak at 9.1 eV, which is not present in our calculations for reasons previously explained. In addition to this, the experimental spectrum show features at 12.0, 12.9, 14.9, 17.4, and 21.8 eV, whereas our calculations show features at 11.3, 12.5, 14.4, 16.6, 19.5, and 22.0 eV respectively. Bortz and French [30] also observed a peak at 32 eV, as do we in our calculations. This last peak arises from interband transitions from the lower valence band (LVB) O 2s states to the antibonding O 2p states. The calculated and experimental optical conductivities are plotted in figure 7. The measured conductivity is generally higher than the calculated one. Our calculations show two main

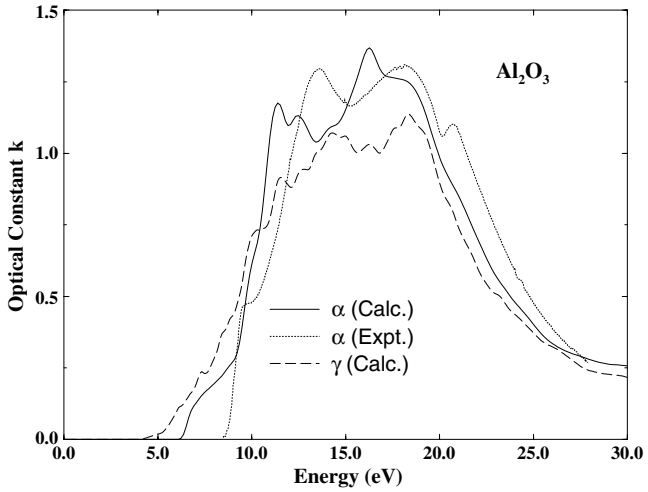

Figure 5. Calculated and experimental optical constant, k, for α- and γ-Al_2O_3.

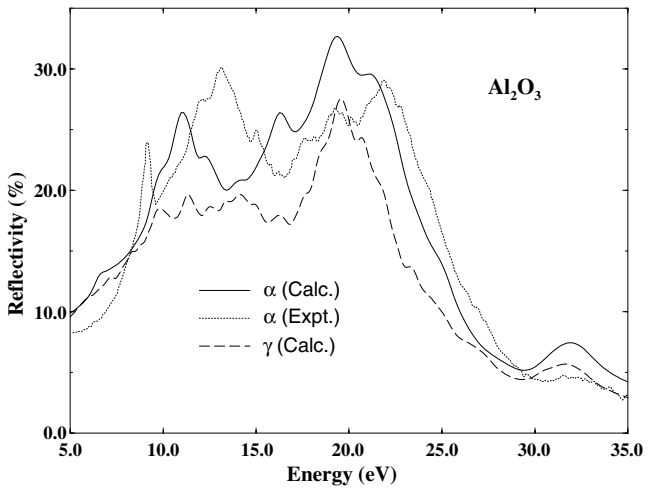

Figure 6. Calculated and experimental reflectivity (%) for α- and γ-Al_2O_3.

features at 11.5, 12.4, 14.5, 16.5, 17.4, and 30.5 eV whereas the measured spectrum shows an excitonic feature at 9.1 eV and other features at 12.4, 13.2, 14.5, 17.4 and 31.5 eV. Thus, a good general agreement between the calculated and measured spectra has been obtained.

4. Conclusions

Results for the electronic and optical properties of the γ and α phases of aluminium oxide have been calculated within DFT. As far as the γ phase is concerned, our results for the optical properties are predictions, and we welcome experiments to verify them. For the α phase we have further made a detailed comparison between our calculated optical properties and the measured spectra from two different experiments. Our calculated values for the ordinary refractive index and static dielectric functions are in good agreement with experiment.

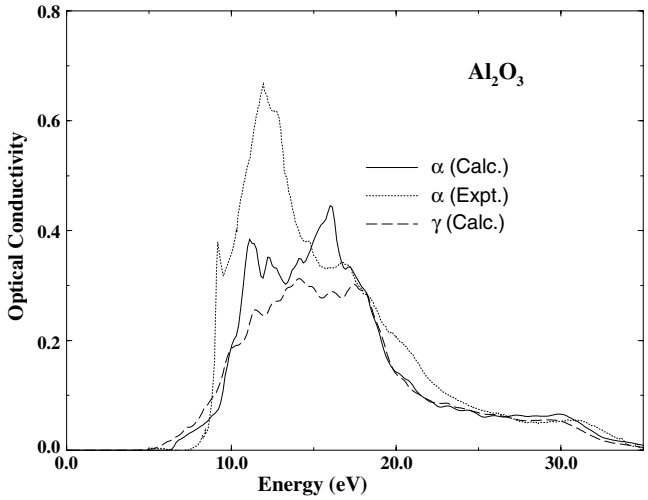

Figure 7. Calculated and experimental optical conductivity for α- and γ-Al_2O_3.

However, the remaining discrepancy between the calculated and experimental dielectric functions is somewhat unsatisfactory. A remedy for this would be to take excitonic effects into consideration. Despite this fact, out numerous comparisons with experimental results for α-alumina suggest that our calculated results for the γ phase should be of a high predictive value.

Acknowledgments

We are grateful to the Swedish Natural Science Research Council (VR), EXCITING (EU), SSF (Atomics), the Brazilian National Research Council (CNPq) and the Japanese Society for the Promotion of Science for financial support. We are also grateful to J M Wills for letting us use his FPLMTO code. WYC was supported by the US DOE under grant No DE-FG02-84ER45170.

References

[1] Hansson P, Halvarsson M and Vuorinen S 1995 *Surf. Coat. Technol.* **76/77** 256 and references cited therein
[2] Verwey E J W 1935 *Z. Kristallogr.* **91** 317
[3] Mo S D, Xu Y N and Ching W Y 1997 *J. Am. Ceram. Soc.* **80** 1193
[4] Streitz F H and Mintmire J W 1999 *Phys. Rev.* B **60** 773
[5] Yourdshahyan Y, Ruberto C, Bengtsson L and Lundqvist B I 1997 *Phys. Rev.* B **56** 8553
Holm B, Ahuja R, Yourdshahyan Y, Johansson B and Lundqvist B I 1999 *Phys. Rev.* B **59** 12777
[6] Ollivier B, Retoux R, Lacorre P, Massiot D and Ferey G 1997 *J. Mater. Chem.* **7** 1049
[7] Sohlberg K, Pennycook S J and Pantelides S T 1999 *Mater. Res. Soc. Symp. Proc.* **549** 165
[8] Wills J M, unpublished
Wills J M and Cooper B R 1987 *Phys. Rev.* B **36** 3809
Price D L and Cooper B R 1989 *Phys. Rev.* B **39** 4945
[9] Hedin L and Lundqvist B I 1971 *J. Phys. C: Solid State Phys.* **4** 2064
[10] Andersen O K 1975 *Phys. Rev.* B **12** 3060
[11] Skriver H L 1984 *The LMTO Method* (Berlin: Springer)
[12] Chadi D J and Cohen M L 1973 *Phys. Rev.* B **8** 5747
Froyen S 1989 *Phys. Rev.* B **39** 3168

[13] Gutierrez G, Taga A and Johansson B 2002 *Phys. Rev.* B **65** 012101
[14] A good description of the calculation of dielectric constants and related properties are found in Gashe T 1993 *Thesis* Uppsala University
[15] Ziman J M 1979 *Models of Disorder* (Cambridge: Cambridge University Press) p 432
[16] Edmonds A R 1974 *Angular Momentum in Quantum Mechanics* (Princeton, NJ: Princeton University Press) p 82
[17] Oppeneer P M, Maurer T, Sticht J and Kübler J 1992 *Phys. Rev.* B **45** 10924
[18] Ahuja R, Auluck S, Wills J M, Alouani M, Johansson B and Eriksson O 1997 *Phys. Rev.* B **55** 4999
[19] Ouyang L and Ching W Y 2001 *J. Am. Ceram. Soc.* **84** 801
[20] O'Brien W L *et al* 1993 *Phys. Rev.* B **47** 140
[21] Dräger G and Leiro J A 1990 *Phys. Rev.* B **41** 12919
[22] Balzarotti A and Bianconi A 1976 *Phys. Status Solidi* b **76** 689
[23] French R H 1990 *J. Am. Ceram. Soc.* **73** 477
[24] Ealet B, Elyakhlouffi M H, Gillet E and Ricci M 1994 *Thin Solid Films* **250** 92
[25] Arakawa E T and Williams M W 1968 *J. Phys. Chem. Solids* **29** 735
[26] Harman A K, Ninomiya S and Adachi S 1994 *J. Appl. Phys.* **76** 8032
[27] Zouboulis E S and Grimsdtich M 1991 *J. Appl. Phys.* **70** 772
[28] Ching W Y and Xu Y-N 1994 *J. Am. Ceram. Soc.* **77** 404
[29] Mo S D and Ching W Y 1998 *Phys. Rev.* B **57** 15219
[30] Bortz M L and French R H 1989 *Appl. Phys. Lett.* **55** 1955
[31] d'Amour H, Schiferl D, Denner W, Schulz H and Holzapfel W B 1978 *J. Appl. Phys.* **49** 4411